Power estimation of a current supplied DBD considering the transformer parasitic elements

Vanesa Rueda, Arnold Wiesner, Rafael Diez, Hubert Piquet

Power Estimation of a Current Supplied DBD Considering the Transformer Parasitic Elements

Vanesa Rueda, *Graduate Student Member, IEEE*, Arnold Wiesner, Rafael Diez, *Senior Member, IEEE*, and Hubert Piquet

***Abstract*—Power estimation of a DBD device supplied by a current source converter is studied in this article, pointing out the prominent contribution of the transformer parasitic elements. The impact of the stray capacitance and magnetizing inductance is stated and an iterative method that estimates the electrical power and DBD waveforms is presented. Results show that the magnetizing inductance can enhance the electrical power without changing the current ratings of the converter and that the stray capacitance must be minimized. Moreover, the experimental results reveal the need for a better DBD model to properly estimate the power. In consequence, an improved model is proposed and validated using a DBD excimer lamp in a wide range of electrical operating conditions.**

***Index Terms*—Current source, dielectric barrier discharge (DBD), electric model, plasma sources.**

I. Introduction

DIELECTRIC barrier discharges (DBD) are efficient non-thermal plasma sources, characterized by the presence of at least one dielectric barrier between the electrodes and the gas. This insulating layer prohibits the evolution to arc regime when the electrical power injected is increased [1]. Additionally, since the electrodes are not in direct contact with the discharge gas (being protected by the dielectric barriers), they are not subjected to wearing or corrosion, increasing the device lifetime [2]. Another very interesting property of DBD is its ability to create spatially homogeneous discharges, which allows uniform treatments [2]. According to these characteristics, many DBD applications can be highlighted as—surface treatment [3], ozone generation [4], biomedical science [5], UV production [6], and decontamination of gases [7]. In this article, DBD excimer lamps are used for experimental purposes. These devices are ultraviolet sources that can produce UV radiation in a very narrow wavelength band (very interesting feature for germicidal processes and skin diseases treatment).

In order to properly design power supplies for DBD applications, there are three important aspects to analyze. The first aspect is the electrical model—DBD are capacitive loads that can be modeled whether using very complex nonlinear equations that describe the DBD electrical and physical behavior [8], [9], or using models as simple as a resistance. The proper selection of the model has a tradeoff between its complexity and the accuracy of its results.

The second aspect is the interaction between the power supply and the DBD process. Several supply waveforms and their impact in DBD applications are reported, voltage-mode sources with sinusoidal or pulsed waveforms are the most common solutions [10], [11]. These two alternatives have been widely compared in the literature, and the operation of DBD under pulsed voltage excitation has shown better results (considering the conversion of electric power to UV emission) [12]. It has also been observed that the discharge under pulsed supply conditions is diffuse and homogeneous [13]—it means that fast changes of the DBD voltage (with short rise time) allow a homogeneous discharge with better performances in the application [14]. However, when pulsed voltage waveforms are imposed, the capacitive nature of the DBD tries to force its own voltage, resulting in current peaks at the voltage edges. The duration and amplitude of these peaks cannot be easily determined since they depend on the rising and falling slopes of the voltage waveform. Therefore, the DBD electric power cannot be easily predicted, and the sizing and design of the power supply generally require oversized devices. On the other hand, the UV radiation has shown to be related to the current injected into the lamp [15]. Therefore, given the capacitive behavior of these devices, it is more suitable to use current-mode converters, that can control the UV and easily adjust the power [15].

Finally, the last aspect concerns the parasitic elements of the power supply components. Those elements may play a crucial role in the definition of the electrical waveforms, and thus strongly impact UV production. Most of the converters for DBD require a step-up transformer that provides the high operating voltage (tens of kV). One of the most relevant parasitic effects in DBD systems is produced by the transformer equivalent capacitance, which draws part of the DBD current and may even

This work was supported in part by the French-Colombian Cooperation Program (ECOS Nord, Colciencias-ICETEX) under Project C16P01 and in part by the Colciencias under Project 294-2016.*(Corresponding author: Vanesa Rueda.)*

V. Rueda and A. Wiesner are with Pontificia Universidad Javeriana, Bo-gota 110231, Colombia and also with LAPLACE Laboratory, Université de Toulouse, CNRS, 31071 Toulouse, France (e-mail: rueda.n@javeriana. edu.co; awiesner@javeriana.edu.co).

R. Diez is with Pontificia Universidad Javeriana, Bogota 110231, Colombia (e-mail: rdiez@javeriana.edu.co).

H. Piquet is with LAPLACE Laboratory, Université de Toulouse, CNRS, 31071 Toulouse, France (e-mail: hubert.piquet@laplace.univ-tlse.fr).

Digital Object Identifier 10.1109/TIA.2019.2933519

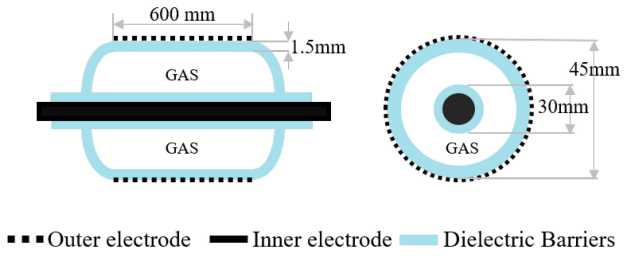

Fig. 1. DBD excimer lamp structure. Lateral and front view.

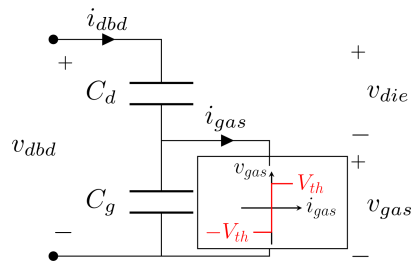

Fig. 2. DBD simplified electrical model.

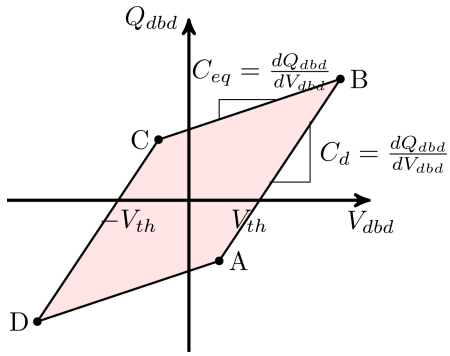

Fig. 3. Example of an ideal charge–voltage Lissajous figure.

prohibit the discharge ignition [16], [17]. In order to avoid this, the step-up transformer can be eliminated [17]–[19], however, the capacitances of the switches and other components may have similar effects [20]. Additionally, elements, such as the transformer magnetizing inductance, L_m, and leakage inductance, L_k, also affect the converter operation, since they resonate with parasitic and DBD equivalent capacitances. Even measurement instruments as voltage probes can alter the supplied waveforms, due to the low equivalent capacitance of DBD.

Analysis of power supplies considering those three aspects can be used to understand the limitations of the converters to obtain desired waveforms (generally, ideal operation minimizing the effects of the parasitic elements). But it can be also used to explore power converters taking advantage of those effects. [21] presents a comprehensive study of the effect of transformer parasitic elements on the performance of the square-shape current source, to decrease the design requirements of the transformer and to increase the power transferred to the lamp. This article is an extension of previous work [21], in which the need for a better DBD model was pointed out, to extend the validity of the analysis in the case of short current pulses. Therefore, the present article aims to provide a more complete and accurate analysis of the square-shape current source with parasitic elements.

This article is organized as follows: First, a review of the classic DBD model is presented in Section II. Then, a description of the experimentation system will be given in Section III. Followed by the power supply analysis with the discussion about the parasitic effects of C_p and L_m. Afterward, in Section V, a comparison between the experimental results and the results is obtained with the classic and improved DBD model and is shown and validated.

II. DBD Electrical Model

DBD can be built using different configurations. The typical structure of a DBD excimer lamp is shown in Fig. 1. It has a cylindrical coaxial geometry made up of quartz. The two concentric dielectric barriers contain a XeCl gas mixture. The inner electrode is a metallic rod, and the outer electrode is a metallic mesh wrapped over the quartz tube (dielectric). The mesh allows the UV to flow outside the lamp. The dimensions of the DBD excimer lamp are given in Fig. 1.

One of the simplest electrical modeling approaches of DBD is the circuit shown in Fig. 2. When the plasma is not ignited, the equivalent circuit is purely capacitive, and it consists of two capacitances connected in series. The C_d capacitance represents the quartz walls, and C_g represents the capacitance of the gas. The equivalent capacitance in this state, is $C_{eq} = (C_g C_d)/(C_g + C_d)$. The sum of the voltages across the gas, v_{gas}, and the dielectric barrier, v_{die}, equals to the DBD voltage, v_{dbd}. The gas discharge is modeled as the conductance, G, in parallel to the capacitance C_g. The gas discharge is obtained when the gas voltage reaches the breakdown voltage, V_{th}. At this point, the gas acquires the behavior of an almost constant voltage source of V_{th} value. In other words, before the gas breakdown ($\mid v_{\text{gas}} \mid < V_{th}$), the DBD is modeled by the capacitance C_{eq}; and after the breakdown, the DBD is modeled by the connection between the capacitance, C_d, and a constant voltage source of $\pm V_{th}$ value (the sign depends on the direction of the current).

The charge–voltage plot (Q–V plot), originally introduced by Manley [22], is a useful tool in the characterization and analysis of DBD. Fig. 3 shows the ideal QV plot of a DBD device. When the plasma is ignited, the Q–V plot forms a parallelogram. Each corner of the parallelogram represents a change of gas state during one full discharge cycle, T. The value of the DBD capacitances and breakdown voltage, V_{th}, can be extracted directly from the parallelogram as shown in Fig. 3 [23]. Additionally, the total energy injected in one cycle is given by the area enclosed by the parallelogram, E_{dbd}, and the total power dissipated can be calculated as the energy divided by the duration of the discharge cycle $P_{\text{dbd}} = E_{\text{dbd}}/T$.

This simplified model gives an insight of the DBD electrical operation, and it has been successfully used for the analysis of different power supplies. For more precise representations, there are complex models including variable conductance models [24], partial discharges [25], and the memory effect [26]. In order to have an initial analysis of the studied power supply, this article will use the model presented in Fig. 2, and then, based on

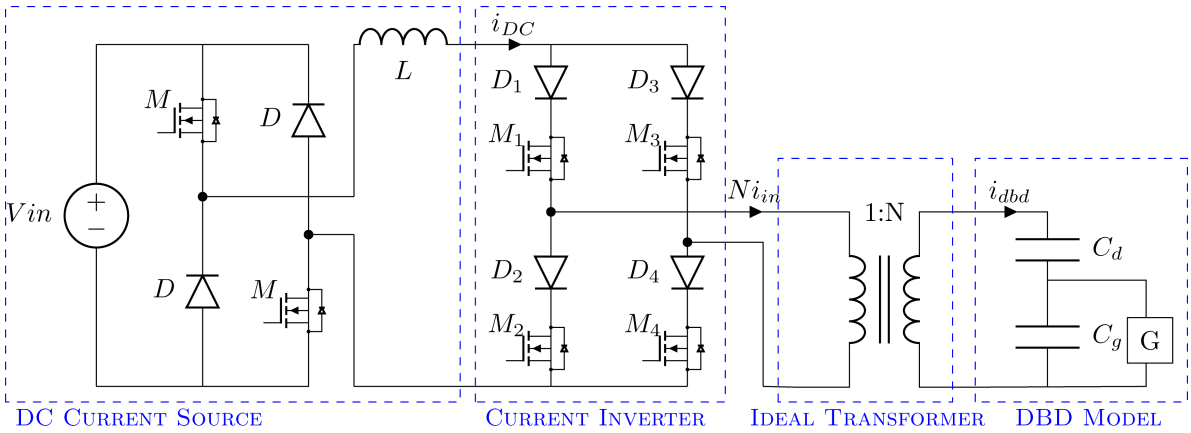

Fig. 4. Topology of the DBD Power Supply.

the experimentation results some modifications will be proposed in section VI.

III. Experimental Setup

The experimentation system consists of a DBD excimer lamp driven by a pulsed current source and a step-up transformer. All the measurement instruments and the power supply are connected to a control interface. The latter can perform automatic parametric sweeps of the power supply variables, recording the results of different operating conditions to simplify the experimentation and the data analysis. The DBD voltage is measured by a 200-MHz digital oscilloscope (LECROY HDO4024) connected through a 1000:1 voltage probe (TESTEC TT-SI 9010), and the current is measured using a current probe (LECROY AP015). The next sections present a detailed explanation of the power supply, operating principle, and the effects of the transformer parasitic elements.

IV. Pulsed Current Source

To provide square current pulses, controlled in frequency, f, amplitude, J, and duty cycle, d, the power supply presented in Fig. 4 was proposed by [27]. The power supply consists of a dc current source, implemented with a two-quadrant chopper, connected in cascade with an H-bridge current inverter. With this topology, the current amplitude, J, is controlled by the dc current source and the frequency, f, and duty cycle, d, by the inverter.

A. Ideal Operation

Fig. 5 shows the operation waveforms of the converter connected to the lamp, without taking into account the transformer stray capacitance C_p, and magnetizing inductance, L_m. As no parasitic elements are considered in this initial analysis, and the DBD waveforms and power is only controlled by the three degrees of freedom (J, d, f), it will henceforward be referred as the ideal operation.

Because of the capacitive character of the DBD, in the ideal operation of the current-mode supply, the slopes of the voltage of the gas, v_{gas}, and dielectric, v_{die}, can be calculated using

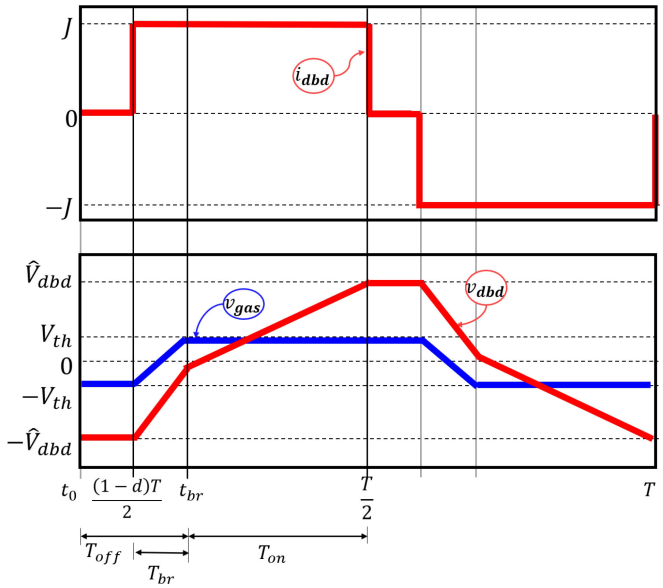

Fig. 5. Ideal operation waveforms.

the injected current and the model of Fig. 2. Accordingly, an expression for the DBD power can be easily deduced, as a function of the three degrees of freedom (f, d, and J)

$$P_{\text{dbd}} = JdV_{th} - 4fC_gV_{th}^2. \tag{1}$$

The duration of the discharge, T_{on}, is calculated in (2), as the current pulse duration minus the time it takes to produce the gas breakdown, T_{br}. Those times can also be deduced using the slopes of the voltages in Fig. 5.

$$T_{on} = \frac{dT}{2} - T_{br} \text{ where } T_{br} = \frac{2V_{th}C_g}{J}. \tag{2}$$

A detailed explanation of the working principle of the two cascaded converters is presented in [27]. To achieve the gas breakdown, a high enough voltage must be applied to the lamp (several kV). However, as the current source cannot withstand the required voltage, a step-up transformer with a winding ratio of 1:10 is required. The dc current source can deliver up to 14 A, in such a way, a maximum of 1.4 A and 7 kV across the DBD load can be generated. The frequency can be varied from 30

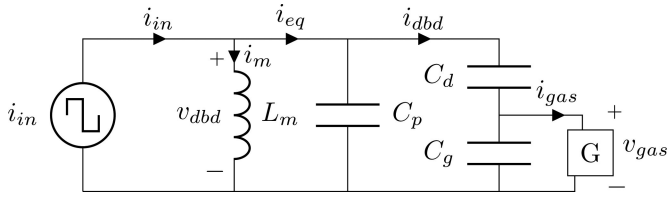

Fig. 6. Equivalent circuit of the pulsed current source with parasitic elements, seen in the transformer's secondary winding.

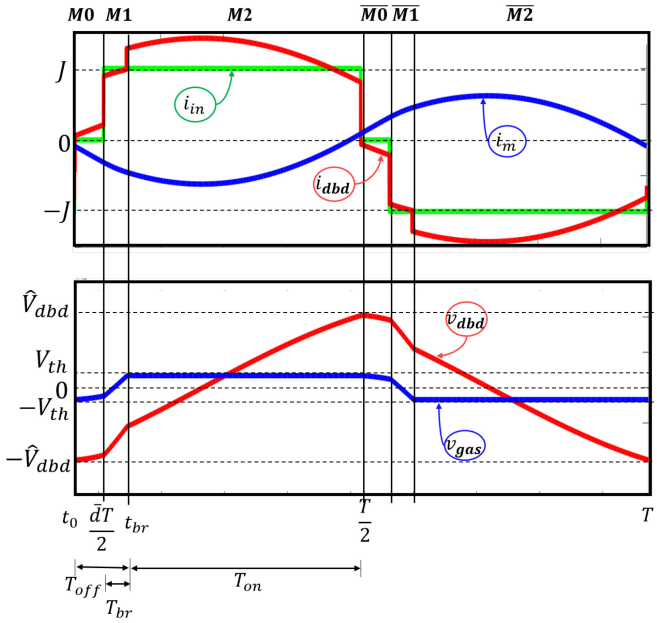

Fig. 7. Nonideal waveforms.

to 200 kHz and the current pulse duration between 300 ns and 10 μs.

B. Operation With Parasitic Elements

The transformer and its parasitic components introduce additional elements into the converter, altering its ideal behavior. Fig. 6 shows the equivalent schematic of the square shape current source connected to the lamp through the nonideal transformer. A parallel resonant circuit is established between the magnetizing inductance, the self-capacitance, and the equivalent capacitance of the lamp.

The lamp waveforms considering the parasitic elements are shown in Fig. 7 and can be compared to the ideal ones, shown in Fig. 5. As can be seen, by including the transformer model, the behavior of the converter in the first half cycle can be described by three operating intervals ($M0, M1, M2$), depicted in Fig. 8. The second half cycle is symmetric to the first one and can be analyzed by analogy ($\overline{M0}, \overline{M1}, \overline{M2}$).

Given that the magnetizing inductance appears as a parallel branch, the current i_{eq} is equal to the input current (ideal square current), i_{in} , minus the magnetizing current i_m. Therefore, during the interval $M0$, $-i_m$ continues flowing through the lamp even though the input current, i_{in}, is null (relaxation time). And in the intervals $M1$ and $M2$, i_{eq} is increased by $-i_m$.

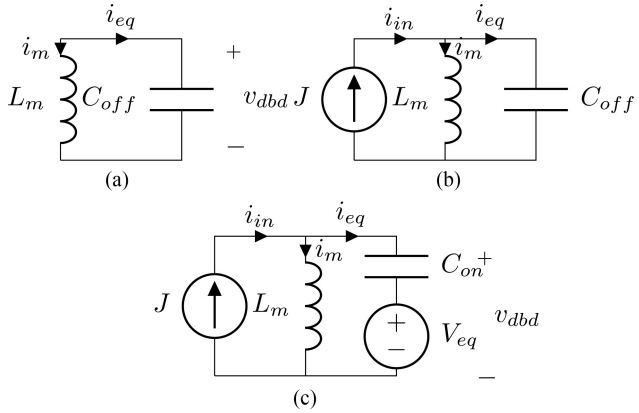

Fig. 8. Equivalent circuits of operating intervals. (a) Operating Interval M0. (b) Operating Interval M1. (c) Operating Interval M2.

i_{eq} represents the sum of currents flowing through the lamp and C_p. Accordingly, the lamp current can be determined, considering a variable capacitive current divider. Before the ignition ($M0$ and $M1$), the current divider is defined by C_p and $C_{eq} = (C_d C_g)/(C_d + C_g)$. Once the lamp is ignited at t_{br}, the current divider between C_p and C_d determines the current available to hold up the discharge and to transfer power into the gas ($M2$).

The graphical state-plane technique can be used to analyze the resonant behavior of the current source for each operating interval. A detailed analysis using this technique is presented in [21]. However, due to the complex nonlinear relationships between the duration of the operating intervals, it is not possible to obtain a closed-form equation to describe the converter using this method, therefore numerical methods are required. A description of each operating interval is presented as follows.

1) Relaxation time, $M0$: At the end of the negative current pulse, the lamp is turned OFF, its voltage reaches the peak value $-\hat{V}_{\text{dbd}}$ and the relaxation time starts. Due to the resonance, the magnetizing current charges C_g, C_d, and C_p simultaneously. Thus, the lamp voltage does not remain constant as in the ideal case. The equivalent circuit of the interval is presented in Fig. 8(a). The resonance frequency is given by

$$w_{off} = \frac{1}{\sqrt{L_m C_{off}}}, \text{ where } C_{off} = C_p + C_{eq}. \quad (3)$$

2) Before breakdown, $M1$: At $t = (1-d)T/2$ the current pulse is injected, but the lamp remains OFF during the T_{br} time. Between the intervals $M0$ and $M1$, v_{gas} is completely inverted from $-V_{th}@t_0$ to $V_{th}@t_{br}$ when the gas breakdown occurs.
3) After breakdown, $M2$: Once the lamp is ignited, it is modeled by the dielectric capacitance, Cd, in series with a V_{th} voltage source (the sign is defined by the current direction). As the lamp is connected in parallel to Cp, the circuit can be reduced to its Thevenin equivalent circuit as shown in Fig. 8(c), where V_{eq} and C_{on} are

$$V_{eq} = V_{th}\frac{C_d}{C_d + C_p} \text{ and } C_{on} = C_d + C_p. \quad (4)$$

Due to the change of the equivalent capacitance of the lamp, the resonance frequency must be redefined as $w_{on} = 1/\sqrt{L_m C_{on}}$. This operating interval finishes when the current pulse ends, it means that $T_{br} + T_{on} = \frac{dT}{2}$.

V. Effects of the Elements of the Transformer

Numerical analysis is proposed to find the solution of the output waveforms under the effects of the parasitic elements. An iterative method to successively find better approximations of the DBD waveforms is proposed. This method starts with the ideal DBD voltage waveform (without the transformer effects), v_{dbd}, to calculate the magnetizing current of the first iteration in the following:

$$i_{m,n} = \frac{1}{L}\int v_{\text{dbd},n-1}dt \tag{5}$$

where n is the iteration number.

Once the magnetizing current has been calculated, the DBD current can be deduced using current divider formed between the parasitic capacitance and the DBD

$$i_{dbd,n} = \begin{cases} \dfrac{(i_{in} - i_{m,n})C_{eq}}{C_{eq} + C_p} & \text{before breakdown} \\ \dfrac{(i_{in} - i_{m,n})C_d}{C_d + C_p} & \text{after breakdown} \end{cases}. \tag{6}$$

Then, $i_{dbd,n}$ is used to solve the equations of the DBD model (8) and (9), and thus, to find the DBD voltage and DBD power

$$v_{\text{gas},n} = \begin{cases} \dfrac{1}{C_g}\displaystyle\int i_{\text{dbd},n}dt & \text{before breakdown} \\ \pm V_{th} & \text{after breakdown} \end{cases} \tag{7}$$

$$v_{\text{die},n} = \frac{1}{C_d}\int i_{\text{dbd},n}dt \tag{8}$$

$$v_{dbd,n} = v_{\text{gas},n} + v_{\text{die},n}. \tag{9}$$

These operations are recursively executed until the calculation of the DBD power converges. The numerical analysis is implemented in Matlab in order to achieve a fast estimation of the converter behavior [28]. Compared to simulation, with this method one can perform sweeps of supply and lamp parameters, using only a few iterations for the convergence. With a circuit solver, the simulation time required to get the steady state is much higher than the iterations used in our method. The resulting waveforms are compared with experimental results in the following sections.

A. Effects of the Magnetizing Inductance

Using the proposed method, the lamp power is calculated for three different duty cycles, d, at a fixed current intensity, J, and frequency, f, considering a large range of L_m values. Fig. 9 shows the results, the dotted lines show the ideal power of the lamp (1). If the magnetizing inductance is large enough, the output power is close to the ideal case and its effects can be neglected. As the inductance decreases, the resonance frequency gets higher and closer to the switching frequency, f, increasing

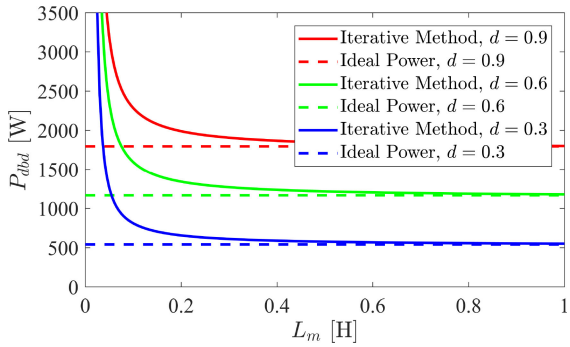

Fig. 9. Effects of Lm at $C_p = 1\ pF$, $C_d = 299\ pF$, $C_g = 119\ pF$, $V_{th} = 1740\ V$, $J = 1.2\ A$, $f = 60kHz$ A $N = 10$.

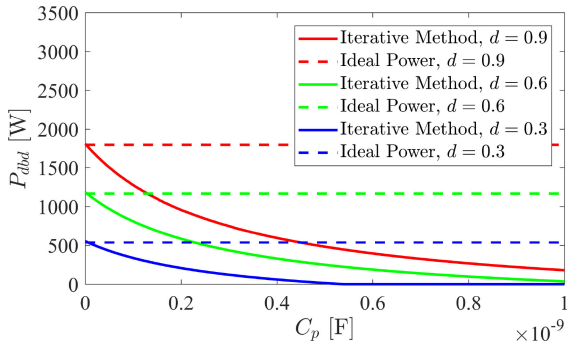

Fig. 10. Effects of Cp at $L_m = 1\ H$, $C_d = 299\ pF$, $C_g = 119\ pF$, $V_{th} = 1740\ V$, $J = 1.2\ A$, $f = 60$ kHz, $N = 10$.

the magnetizing current and output power. In such a way, properly handled, a small magnetizing inductance can be used to increase the DBD power and reduce the size of the transformer.

As the magnetizing current charges the gas capacitance during the relaxation time, if this current is high enough, it could cause the ignition of the lamp even before the injection of the current pulse. Thus, in this mode, the ON time would be mostly controlled by the magnetizing current and not by the input current, i_{in}.

B. Effects of the Transformer Capacitance

Fig. 10 shows the effects of C_p in the output power for a fixed operating point and a high magnetizing inductance. As was previously explained, the parasitic capacitance draws part of the current i_{eq}, decreasing the injected current and power to the DBD. When C_p is comparable to the lamp equivalent capacitance, those effects are strong and they might even affect the ignition of the lamp. In order to have the maximum power injected into the lamp, the minimization of the parasitic capacitance of the transformer, and other parasitic capacitances, such as the switches or voltages probes, is necessary. However, given that the magnetizing inductance does not have to be maximized, the design of the transformer is less challenging and the parasitic capacitance can be minimized more easily with a smaller transformer.

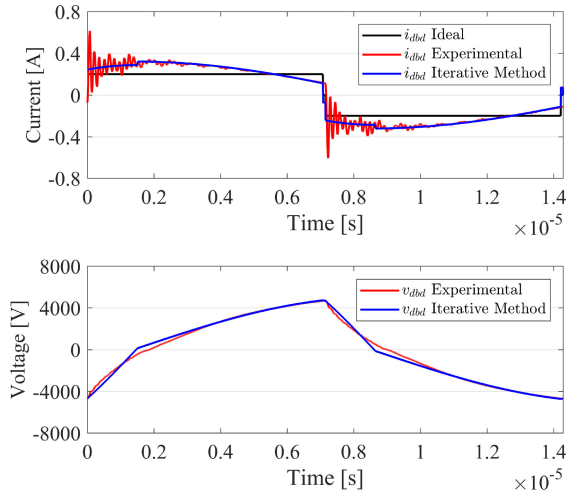

Fig. 11. Operating point $f = 70$ kHz, $J = 0.2\ A$, $d = 1$.

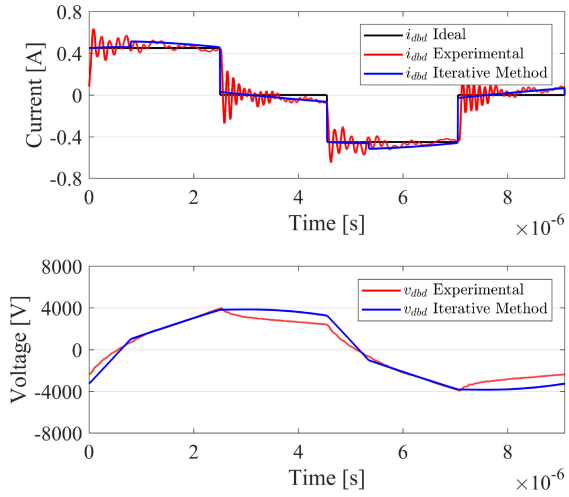

Fig. 12. Operating point $f = 110$ kHz, $J = 0.4\ A$, $d = 0.55$.

VI. Results

To validate the analysis presented in the previous section, experimental waveforms at different operating conditions were studied. The transformer used in the experimental setup has a turns ratio of $N = 10$, a magnetizing inductance of $L_m = 0.08\ H$, and a stray capacitance of $C_p = 16\ pF$. And the DBD excimer lamp parameters are: $C_d = 299\ pF$, $C_g = 119\ pF$, and $V_{th} = 1740\ V$. The parameter of the transformer and DBD were used in the analysis of all the numerical methods here presented. Figs. 11 and 12 present two of the studied operating points. The red lines show the experimental current and voltage of the DBD, and the blue lines show the waveforms calculated with the numerical method exposed previously. As can be seen in Fig. 11, the voltage and current waveforms are similar to the experimental ones. This operating point is characterized by a high duty cycle. Under this condition, the proposed analysis works properly. However, when the duty cycle is reduced, the analysis is less accurate. Fig. 12 presents one operating point obtained under such conditions. As can be seen, after the current pulse ends, the experimental lamp voltage decreases rapidly,

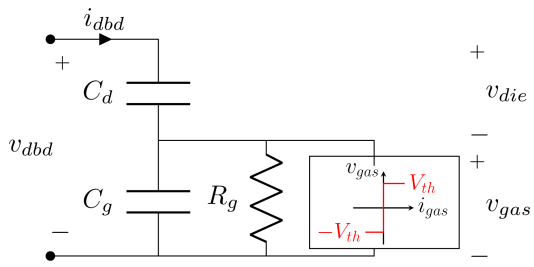

Fig. 13. Improved DBD electrical model.

while the calculated waveforms remain almost constant, creating a noticeable difference between them. This problem is not associated with the analysis here presented, but with the accuracy of the DBD electrical model used. Furthermore, high-frequency oscillations in the measured DBD current can be seen, these are mainly caused by a resonance between the leakage inductance of the transformer and the equivalent capacitance of the DBD and parasitic elements.

In order to have a better approximation, an improved model is presented in Fig. 13. As can be seen in the experimental DBD voltage of Fig. 12, the voltage drop tends to a negative exponential, therefore, a resistor in parallel to the gas conductance is included. The identification of the improved model parameters, $[C_d, C_g, V_{th}, R_g]$, uses the Q–V plot to obtain an initial set of parameters based on the parallelogram (initial conditions) and then performs a grey-box identification.

In the grey-box identification, the structure of the model (Fig. 13) and one observable state (DBD voltage, v_{dbd}) are known. In this way, the problem seeks to find the best set of parameters to approximate the observable state [29]. This can be formulated as an optimization problem which objective function minimizes the norm of the quadratic error between the experimental DBD voltage, v_{dbdEXP}, and the estimated voltage, v_{dbdEST}. The estimated DBD voltage is obtained solving the differential equations of the improved model (10)–(12), with the experimental current, i_{dbdEXP}, as input

$$\begin{aligned} C_g \frac{dv_{\text{gas}}}{dt} + \frac{v_{\text{gas}}}{R_g} &= i_{dbd}, \quad \text{before breakdown} \\ v_{\text{gas}} &= \pm V_{th}, \quad \text{after breakdown} \end{aligned} \tag{10}$$

$$C_d \frac{dv_{\text{die}}}{dt} = i_{dbd} \tag{11}$$

$$v_{dbd} = v_{\text{gas}} + v_{\text{die}}. \tag{12}$$

To solve this optimization problem, the minimization of the error with respect to the set parameters has to be done iteratively. The objective of each iteration is to find the disturbance to the parameters that reduce the objective function. The Levenberg–Marquardt gradient algorithm was used to find the DBD parameters [30]. After using the grey-box identification, the obtained parameters of the model were: $C_g = 248\ pF$, $C_d = 73\ pF$, $V_{th} = 1600\ V$, and $R_g = 2900\ \Omega$. These values are used henceforth in the analysis of the converter with the improved model.

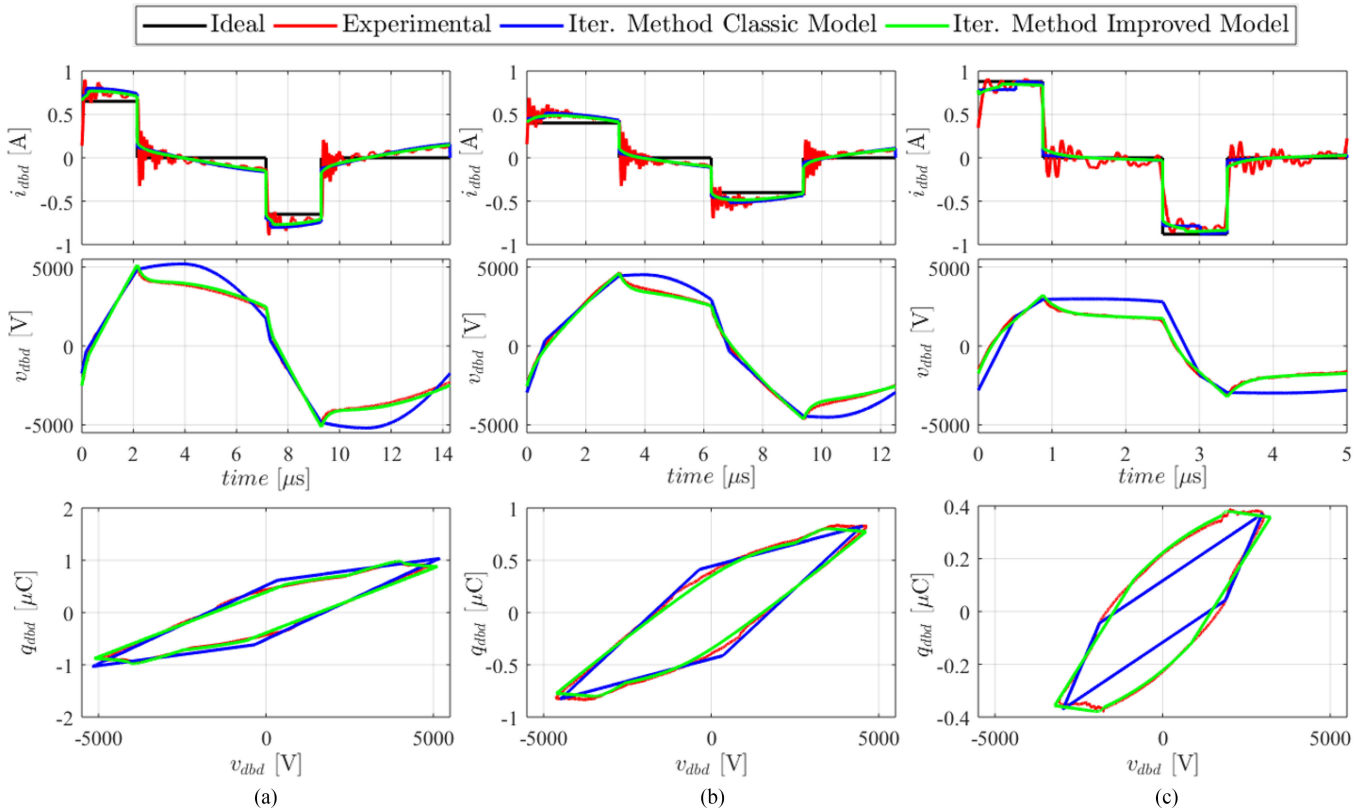

Fig. 14. DBD waveforms for different operating points. (a) $f = 70$ kHz, $J = 0.6$ A, $d = 0.3$ (b) $f = 80$ kHz, $J = 0.4$ A, $d = 0.5$ (c) $f = 200$ kHz, $J = 0.8$ A, $d = 0.35$.

TABLE I
POWER COMPARISON

Operating Point	Exp. Power [W]	Ideal Power [W]	Classic Model [W]	Impro. Model [W]
$f = 70kHz, J = 0.2A, d = 1$	314	247	333	324
$f = 110kHz, J = 0.5A, d = 0.55$	351	272	322	352
$f = 70kHz, J = 0.6A, d = 0.3$	357	238	400	360
$f = 80kHz, J = 0.4A, d = 0.5$	359	233	344	353
$f = 200kHz, J = 0.8A, d = 0.35$	374	248	227	376

On the other side, the analysis of the square current source with parasitic elements, using the improved model, can be performed with the same method previously presented (Section V). However, the gas voltage calculation, (8), must be replaced by (10).

Fig. 14 shows the results of three operating waveforms using both models. Red waveforms represent the experimental results, blue waveforms represent the numerical method using the classic model, and green waveforms represent the numerical method using the improved model. Additionally, the Q–V plot is included to compare the energy delivered to the lamp of each approximation (area enclosed by the parallelogram). In those figures, it can be seen that the improved model obtains better approximations of the DBD voltage than the classic model.

Additionally, Table I compares the values of the experimental power, the ideal power calculated with (1), the power obtained by the classic model, and the power obtained by the improved model for five different operating points. The first two operating points correspond to Figs. 11 and 12, and the following three correspond to Fig. 14.

As can be seen in Table I, there is a big difference between the ideal power (calculated without parasitic elements), and the experimental power. This can be explained by the model error, as well as, by the increase of the lamp current caused by the magnetizing inductance, as was previously mentioned. This proves that the DBD power can be highly enhanced without changing the ratings of the current source, but only through the design of a transformer with an appropriate magnetizing inductance. Furthermore, given that the stray capacitance is related to the number of turns of the transformer, a smaller transformer, with a smaller magnetizing inductance will decrease C_p, achieving even better performances.

Finally, there is a noticeable enhancement in the accuracy of the DBD power estimation using the improved model. At high frequencies (last row of Table I), the effects of the parasitic elements are weak, therefore, the differences between the ideal power and the experimental power are mostly given by the error of the DBD model. At this point, as well as at low frequencies, better results are obtained with the improved model. The improved model proposed in this article has only been proven using DBD excimer lamps and a square-current source, however, DBD setups with Q–V plots characterized by an almond shape as Fig. 14.(c) could make use of it. Further analysis of the characterization and use of the

model with different DBD devices and supply waveforms is required.

VII. Conclusion

The analysis of the square current source, considering the effects of the parasitic capacitance and magnetizing inductance is presented and a numerical method is proposed and validated for finding the operating ratings and waveforms of the converter.

It is proven that the magnetizing inductance can be used to enhance the power delivered to the lamp, while the parasitic capacitance decreases it. Higher powers can be attained with small magnetizing inductance without changing the current source ratings. Moreover, without the restriction of the maximization of the inductance, smaller transformers can be used with smaller parasitic capacitances.

Very low values of magnetizing inductance can cause the ignition of the lamp before the current pulse, changing the operating mode of the converter.

The need for a more complex model for the DBD was raised in order to have better approximations of the electrical power and ratings of the converter at every operating point. An improved model is presented and validated under different operation conditions.

References

[1] U. Kogelschatz, "Dielectric-barrier discharges: Their history, discharge physics, and industrial applications," *Plasma Chem. Plasma Process.*, vol. 23, no. 1, pp. 1–46, Mar. 2003.

[2] R. Brandenburg, "Dielectric barrier discharges: progress on plasma sources and on the understanding of regimes and single filaments," *Plasma Sources Sci. Technol.*, vol. 26, no. 5, Mar. 2017, Art. no. 053001.

[3] G. Borcia, C. A. Anderson, and N. M. D. Brown, "Dielectric barrier discharge for surface treatment: Application to selected polymers in film and fibre form," *Plasma Sources Sci. Technol.*, vol. 12, no. 3, 2003, Art. no. 335.

[4] U. Kogelschatz, *Advanced Ozone Generation*. Boston, MA, USA: Springer, 1988, pp. 87–118.

[5] G. Fridman, G. Friedman, A. Gutsol, A. B. Shekhter, V. N. Vasilets, and A. Fridman, "Applied plasma medicine," *Plasma Process. Polym.*, vol. 5, no. 6, pp. 503–533, 2008.

[6] M. Lomaev, E. Sosnin, and V. Tarasenko, "Excilamps and their applications," *Progr. Quantum Electron.*, vol. 36, no. 1, pp. 51–97, 2012.

[7] K. Skalska, J. S. Miller, and S. Ledakowicz, "Trends in NOX abatement: A review," *Sci. Total Environ.*, vol. 408, no. 19, pp. 3976–3989, 2010.

[8] A. A. El-Deib, F. Dawson, S. Bhosle, and G. Zissis, "Circuit-based model for a dielectric barrier discharge lamp using the finite volume method," *IEEE Trans. Plasma Sci.*, vol. 38, no. 9, pp. 2260–2273, Sep. 2010.

[9] S. Liu and M. Neiger, "Electrical modelling of homogeneous dielectric barrier discharges under an arbitrary excitation voltage," *J. Phys. D: Appl. Phys.*, vol. 36, no. 24, pp. 3144–3150, Nov. 2003.

[10] R. P. Mildren, R. J. Carman, and I. S. Falconer, "Visible and VUV emission from a xenon dielectric barrier discharge using pulsed and sinusoidal voltage excitation waveforms," *IEEE Trans. Plasma Sci.*, vol. 30, no. 1, pp. 192–193, Feb. 2002.

[11] K. Kyrberg, H. Guldner, A. Rupp, and O. Schallmoser, "Half-bridge and full-bridge choke converter concepts for the pulsed operation of large dielectric barrier discharge lamps," *IEEE Trans. Power Electron.*, vol. 22, no. 3, pp. 926–933, May 2007.

[12] U. Kogelschatz, "Industrial innovation based on fundamental physics," *Plasma Sources Sci. Technol.*, vol. 11, no. 3A, pp. A1–A6, 2002.

[13] X. Lu and M. Laroussi, "Temporal and spatial emission behaviour of homogeneous dielectric barrier discharge driven by unipolar sub-microsecond square pulses," *J. Phys. D: Appl. Phys.*, vol. 39, no. 6, pp. 1127–1131, 2006.

[14] R. P. Mildren and R. J. Carman, "Enhanced performance of a dielectric barrier discharge lamp using short-pulsed excitation," *J. Phys. D: Appl. Phys.*, vol. 34, no. 1, pp. L1–L6, Dec. 2000.

[15] H. Piquet, S. Bhosle, R. Diez, and M. V. Erofeev, "Pulsed current-mode supply of dielectric barrier discharge excilamps for the control of the radiated ultraviolet power," *IEEE Trans. Plasma Sci.*, vol. 38, no. 10, pp. 2531–2538, Oct. 2010.

[16] D. Florez, X. Bonnin, R. Diez, and H. Piquet, "Impact of the transformer in the current mode supply of dielectric barrier discharge excimer lamps," in *Proc. Brazilian Power Electron. Conf.*, 2013, pp. 1171–1176.

[17] M. Meisser, R. Kling, and W. Heering, "Transformerless high voltage pulse generators for bipolar drive of dielectric barrier discharges," in *Proc. PCIM Power Electron. Conf.*, 2011, pp. 243–248.

[18] M. A. Diop, A. Belinger, and H. Piquet, "DBD tranformerless power supplies: impact of the parasitic capacitances on the power transfer," *Proc. J. Phys.: Conf. Ser.*, 2017, vol. 825, no. 1, 2017, Art. no. 012004.

[19] A. El-Deib, F. Dawson, and G. Zissis, "Transformer-less current controlled driver for a dielectric barrier discharge lamp using HV silicon carbide (SiC) switching devices," in *Proc. IEEE Energy Convers. Congr. Expo.*, 2011, pp. 1124–1131.

[20] V. Rueda, R. Diez, and H. Piquet, "Optimum transformer turns ratio for the power supply of dielectric barrier discharge lamps," *IET Power Electron.*, vol. 11, no. 1, pp. 62–67, 2018.

[21] V. Rueda, A. Wiesner, R. Diez, and H. Piquet, "Enhancement of the DBD power for current-mode converters using the step-up transformer elements," in *Proc. IEEE Ind. Appl. Soc. Annu. Meet.*, 2018, pp. 1–8.

[22] T. C. Manley, "The electric characteristics of the ozonator discharge," *J. Electrochem. Soc.*, vol. 84, no. 1, pp. 83–96, 1943. [Online]. Available: https://doi.org/10.1149/1.3071556

[23] A. V. Pipa and R. Brandenburg, "The equivalent circuit approach for the electrical diagnostics of dielectric barrier discharges: The classical theory and recent developments," *Atoms*, vol. 7, no. 1, 2019, Art. no. 14.

[24] A. M. Lopez, H. Piquet, D. Patino, R. Diez, and X. Bonnin, "Parameters identification and gas behavior characterization of DBD systems," *IEEE Trans. Plasma Sci.*, vol. 41, no. 8, pp. 2335–2342, Aug. 2013.

[25] F. J. J. Peeters and M. C. M. van de Sanden, "The influence of partial surface discharging on the electrical characterization of DBDS," *Plasma Sources Sci. Technol.*, vol. 24, no. 1, Dec. 2014, Art. no. 015016.

[26] N. Naudé, J.-P. Cambronne, N. Gherardi, and F. Massines, "Electrical model and analysis of the transition from an atmospheric pressure townsend discharge to a filamentary discharge," *J. Phys. D: Appl. Phys.*, vol. 38, no. 4, pp. 530–538, Feb. 2005.

[27] D. Florez, R. Diez, H. Piquet, and A. K. H. Harb, "Square-shape current-mode supply for parametric control of the DBD excilamp power," *IEEE Trans. Ind. Electron.*, vol. 62, no. 3, pp. 1451–1460, Mar. 2015.

[28] *MATLAB*. (2018). MathWorks Inc., 2018.

[29] T. P. Bohlin, *Practical Grey-Box Process Identification: Theory and Applications*, 1st ed. London, U.K.: Springer, 2010.

[30] J. J. More, "The Levenberg-Marquardt algorithm: Implementation and theory," in *Numerical Analysis*, G. A. Watson, Ed., Berlin, Germany: Springer, 1978, pp. 105–116.

Vanesa Rueda (S'11) received the B.Sc. and M.Sc. degrees in electronics engineering from Pontificia Universidad Javeriana, Bogota, Colombia, in 2013 and 2016, respectively. She is currently working toward the Ph.D. degree at the LAPLACE Research Group of the Institut National Polytechnique de Toulouse and Pontificia Universidad Javeriana, Toulouse, France.

Her research interests include the design of power converter for electrical discharges and low-temperature plasma and its applications in gas treatment and UV generation.

Arnold Wiesner received the B.S. and M.Sc. degrees in electronics engineering from Pontificia Universidad Javeriana, Bogota, Colombia, in 2012 and 2013, respectively. He is currently working toward the Ph.D. degree at the Institut National Polytechnique de Toulouse, Toulouse, France.

He is currently an Assistant Professor with the Department of Electronics, Universidad Santo Tomas, Bogota, Colombia. His current research interests include power converters for dielectric barrier discharges and renewable energy systems.

Rafael Dez (M'10–SM'15) received the B.Sc. degree in electronics engineering from Pontificia Universidad Javeriana, Bogota, Colombia, in 2001, the M.Sc. degree in 2005 from Universit Paul Sabatier, Toulouse, France, and the Ph.D. degree in 2008 from the Institut National Polytechnique de Toulouse, Toulouse, France.

He is currently an Associate Professor with the Department of Electronics Engineering, Pontificia Universidad Javeriana, Bogota, Colombia. His current research interests include the design of power converters for electric discharges.

Hubert Piquet was born in Arras, France, in 1960. He graduated in applied physics from the Ecole Normale Suprieure de Cachan, Cachan, France in 1984 and received the Ph.D. degree in electrical engineering from the Institut National Polytechnique de Toulouse, Toulouse, France, in 1990.

He is currently a Professor with Toulouse INP/ENSEEIHT Ing. School. He teaches power electronics and systemic approach in electrical engineering. His current research interests include plasma applications and design of aircraft electrical networks and the investigation takes place in the LAPLACE laboratory, Toulouse, France.